Studies on the nonlinear optical properties of two-step GaAs/Ga$_{1-x}$Al$_x$As quantum well

J C Martínez-Orozco[1] , F Ungan[2] and K A Rodríguez-Magdaleno[1]

[1] Unidad Académica de Física, Universidad Autónoma de Zacatecas, Calzada Solidaridad esquina con Paseo la Bufa S/N, C.P. 98060, Zacatecas, Zac, México
[2] Faculty of Technology, Department of Optical Engineering, Sivas Cumhuriyet University, 58140 Sivas, Turkey

E-mail: jcmartinez@uaz.edu.mx

CrossMark

Abstract

In this paper, the numerical computation for the absorption coefficient and the relative refractive index change, considering the third order correction nonlinear optical properties, is reported. This study was performed for a symmetric two-step GaAs/Ga$_{1-x}$Al$_x$As quantum well, subjected to a constant electric field applied along the growth direction z, and an in-plane constant magnetic field B. We also consider the intense laser field effect, characterized through the laser-dressing parameter α_0. The electronic structure computation was obtained by working under the effective mass approximation and the Schödinger equation was solved by diagonalization procedure. The optical properties are calculated by using the well-established compact density matrix formalism expressions for the nonlinear optical properties of interest. In general, we found that the structural parameters, as the step-like potential or the central barrier, permit the resonant peak and the amplitude design. We also found that the system becomes more sensitive to electric than to magnetic field, and finally that the intense, non-resonant, laser field can strongly change the optical properties of interest. Our results indicate that the implementation of the step-like potential profile, experimentally feasible, enhance the optical properties of interest, that falls within the THz electromagnetic range, and can be used to design a photodetector, or even can be used for quantum cascade lasers design.

Supplementary material for this article is available online

(Some figures may appear in colour only in the online journal)

1. Introduction

Nowadays the high control that can be obtained in the composition and characterization of the III–V heterostructures is continuously improving, for instance Zhang *et al* [1] experimentally investigated the effect of the manipulator temperatures on the uniformity of AlGaAs/GaAs epitaxial layers, grown by molecular beam epitaxy (MBE), and concluded that the uniformity of the AlGaAs/GaAs epitaxial layers, optimizing the manipulator temperature with a higher temperature, was improved. Cetinkaya *et al* [2] experimentally studied the optical properties of n- and p-type GaAsBi/AlGaAs single quantum well (QW) structures in order to determine the effect of the AlGaAs barrier doping, separated by an undoped AlGaAs spacer layer from the GaAsBi active region (QW), on the photoluminescence spectra, and obtained that the bismuth incorporation induced an important shift in the main intra-band transition PL spectra. And just to give another recent reference in this direction Yue *et al* [3] proposed and implemented, with MBE, a type II InGaAs/GaAsBi QW structure for long wavelength emitters of high quality with no In and Bi inter-diffusion between InGaAs and GaAsBi layers. These high control, and sophisticated, semiconductor growth techniques permit to propose promising semiconductor devices such as quantum cascade lasers (QCL) [4, 5]. In particular, the variable barrier height AlGaAs/GaAs

QCL was proposed to operate in the THz electromagnetic spectra region [6], that is just this range of operation that we are interested in for possible device design.

It is worth mentioning that one of the building blocks for semiconductor devices design are, undoubtedly, high quality heterostructures as discussed above, and among the wide quantity of possibilities, the coupled double QW structures, with different shapes and doping profile, are of paramount importance [7–11], because they can be used to tune linear and nonlinear optical properties that can be the intersubband absorption coefficient (AC) [12], the relative refractive index change (RIC) [11], second (third) order harmonic generation and nonlinear optical rectification [9], phase-dependent intersubband optical properties of asymmetric coupled QWs —just to give some examples—as a function of the electric and magnetic field, hydrostatic pressure, barrier doping profiles etc, the coupled double QW can also be used for field effect transistor applications [8, 13]. Even, multiple QWs semiconductor nano-structures are of interest for optical properties, as the intersubband AC, that can be tuned by an applied electric field [14]. In this line, the step-like potential profile [15–20] is an interesting system due to its asymmetry, because of this, in function of its design and used materials, induces wave function asymmetry that can enhance the dipole matrix element meaning that the expectation value of ez ($\langle\psi_i(z)|e\,z|\psi_f(z)\rangle$) increases by the overlapping of the involved wave functions, that can be controllable with intense laser or electromagnetic fields effects [15], plasmon mode coupling in an AlGaAs/GaAs, by means of electric field effects, was also reported by Song *et al* [16], and it was also proposed as a mechanism to generate direct and indirect excitons in InGaN/GaN strained step-like QWs [18].

In addition to the above mentioned effects on QW semiconductor heterostructures, the non-resonant intense laser field (ILF) effect, polarized perpendicularly to the interface, can modify the potential *seen* by the electrons in such a way that even can induce a transition from single to double QW potential profile, characterized through the *laser dressing parameter* α_0, as reported by Lima *et al* [21]. The geometrical parameter α_0 allows to compute the bound-states energy levels for the deformed potential (*laser dressed potential*) seen by the charge carriers in the semiconductor heterostructure. The ILF effect has been studied in several systems, for instance in single $Ga_xIn_{1-x}N_yAs_{1-y}$/GaAs QW [22], considering electromagnetic fields reporting nonlinear optical properties [23], ILF effect on the nonlinear optical properties for a two-level Al_xGa_{1-x}N/GaN single QW [24], and single *n*-type δ-doped QW reporting the same optical properties [25], just to give some examples. But also double QW structures has been also investigated, for instance the electromagnetically induced transparency, due to the laser-induced electron tunneling, for an asymmetric double GaAs/Al_xGa_{1-x}As QW has been reported [26], the ILF effect on the transmission coefficient and on the resonance energy for a resonant tunneling structure was also reported [27]. Even the ILF effect, on the electronic structure, has been studied for an GaAs/Al_xGa_{1-x}As superlattice [28].

In this paper, we are interested in an Al_xGa_{1-x}As/GaAs double symmetric step-like potential profile. In particular, we present the AC and the relative RIC, considering nonlinear corrections up to third order, when the system is subjected to an electric field (E) along the growth direction, to an in-plane magnetic field (B) and to a non-resonant ILF effect. These external factors allow to manipulate the optical properties and also the proposed step-like potential profile has an important effect on the optical properties as will be shown below.

The organization of the paper is as follows: section 2 presents the description of the theoretical framework. In section 3 the results and discussion section is presented. Finally, section 4 contains the main conclusions of the study.

2. Theoretical framework

The effective mass approximation has been demonstrated to be an accurate way to deal with the electronic structure computation of semiconductor quantum heterostructures. In this case, we are considering a symmetric two-step GaAs/$Ga_{1-x}Al_x$As rectangular QW when the effect of electric field, magnetic field and non-resonant ILF effect, are considered. The one-dimensional effective mass Hamiltonian is given by:

$$H = \left[-\frac{\hbar^2}{2\,m_e^*}\frac{d^2}{dz^2} + \frac{(q\,B)^2}{2\,m_e^*}z^2 + zeF + \langle V(z;\,\alpha_0)\rangle \right], \quad (1)$$

here m_e^* is the electron effective mass, F represents the strength of the *z*-oriented applied electric field, the in-plane (*x*-oriented) static applied magnetic field, characterized by a vector potential $\vec{A} = -Bz\hat{i}$, gives the well known parabolic potential term. The laser-dressed potential $\langle V(z;\,\alpha_0)\rangle$ is:

$$\langle V(z;\,\alpha_0)\rangle = \frac{\Omega}{2\pi}\int_0^{2\pi/\Omega} V_c(z + \alpha_0\sin\Omega t)dt, \quad (2)$$

where the *laser-dressing parameter* α_0 is:

$$\alpha_0 = \frac{eA_0}{m_e^*\Omega}, \quad (3)$$

A_0 representing the optical field strength and Ω stands for the non-resonant frequency of the laser field, e is the absolute value of the electron charge and the two-step GaAs/$Ga_{1-x}Al_x$As QW confining potential is given by:

$$V_c(z) = \begin{cases} V_0, & z < -z_3 \\ V_s, & -z_3 \leqslant z < -z_2 \\ 0, & -z_2 \leqslant z < -z_1 \\ V_{cb}, & -z_1 \leqslant z < z_1 \\ 0, & z_1 \leqslant z < z_2 \\ V_s, & z_2 \leqslant z < z_3 \\ V_0, & z > z_3 \end{cases} \quad (4)$$

where V_x is the band discontinuity calculated by $V_x = Q_c(1155x + 370x^2)$ meV, with $Q_c = 0.6$ that represents the conduction band offset parameter for GaAs/$Ga_{1-x}Al_x$As QW, x is the Al concentration in each region. L_w, L_{cb}, L_s denote the well, the central barrier and step barrier widths,
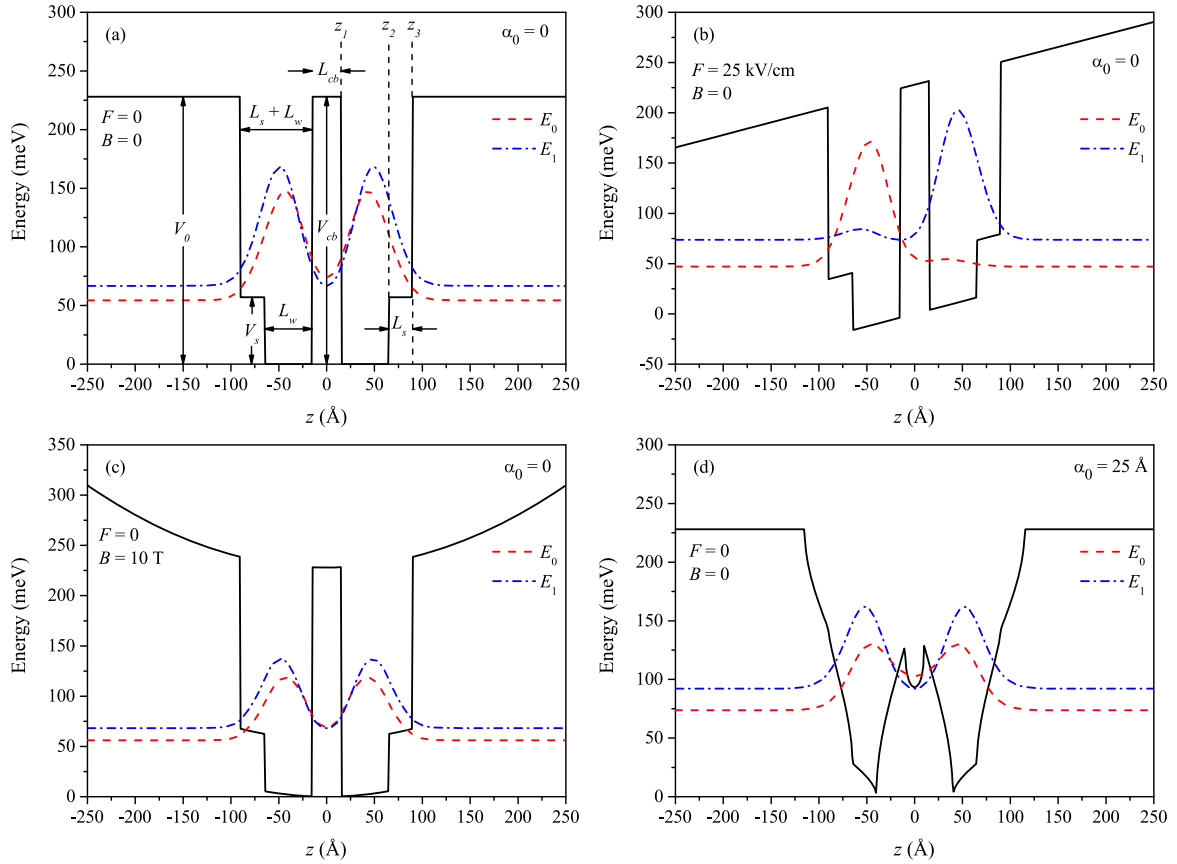
Figure 1. Potential profile, and the first two level probability densities, for a two-step GaAs/Ga$_{1-x}$Al$_x$As QW: (a) without any external interaction, (b) with an applied electric field of strength 25 kV cm^{-1}, (c) a static magnetic field of 10 T, and finally (d) with a laser-dressing parameter $\alpha_0 = 25$ Å. The Al concentration x determinate the barrier height and L_w, L_{cb}, L_s stands for the well, central barrier and step barrier widths, respectively.

respectively, with $z_1 = L_{cb}/2$, $z_2 = L_{cb}/2 + L_w$, and $z_3 = L_{cb}/2 + L_w + L_s$, see figure 1(a) for a graphical representation of the potential profile.

The electronic structure computation was performed within the framework of the effect mass and parabolic band approximation. Here, we implemented a well proved diagonalization numerical scheme, in order to solve Schrödinger equation with hamiltonian (1), that has been used to study the electronic structure for an important amount of semiconductor quantum nanostructures, for instance see [7, 9, 12] and references therein, in fact this is an in-house developed program code adapted to each system instead of using commercial software. This is done by the diagonalization of the Hamiltonian matrix H_{mn} that comes from the envelope's wave functions expansion for the Hamiltonian in terms of the complete set of wave functions of an infinite barrier potential well of width L. The laser-dressing potential given by the equation (2), which depends on the laser-dressing parameter α_0, is numerically integrated to obtain the potential profile *seen* by the confined electrons. Then, by working under the envelope function approximation, we diagonalize the computed the Hamiltonian matrix to solve the eigenvalues problem. Then, the refractive index and optical AC changes, for the two-step GaAs/Ga$_{1-x}$Al$_x$As QW structure, can be easily computed with the help of the density-matrix approach

method that provides us analytical expressions for the linear optical ACs and the RICs [11, 15], given by:

$$\beta^{(1)}(\omega) = \omega \sqrt{\frac{\mu_0}{\varepsilon_0\,\varepsilon_r}} \left[\frac{\rho\;\hbar\;\Gamma_{10}|M_{10}|^2}{(E_{10} - \hbar\;\omega)^2 + (\hbar\;\Gamma_{10})^2} \right]. \quad (5)$$

$$\frac{\Delta n^{(1)}(\omega)}{n_r} = \frac{\rho\;|M_{10}|^2}{2\,n_r^2\,\varepsilon_0} \left[\frac{E_{10} - \hbar\;\omega}{(E_{10} - \hbar\;\omega)^2 + (\hbar\;\Gamma_{10})^2} \right], \quad (6)$$

while the third-order nonlinear optical ACs is given by:

$$\beta^{(3)}(\omega, I) = -\sqrt{\frac{\mu_0}{\varepsilon_0\varepsilon_r}} \left(\frac{\omega\,I}{2n_r\varepsilon_0 c} \right)$$

$$\frac{\rho\;\hbar\Gamma_{10}|M_{10}|^2}{[(E_{10} - \hbar\omega)^2 + (\hbar\Gamma_{10})^2]^2} \{4|M_{10}|^2$$

$$- \frac{|M_{11} - M_{00}|^2 [3E_{10}^2 - 4E_{10}\hbar\omega + \hbar^2(\omega^2 - \Gamma_{10}^2)]}{E_{10}^2 + (\hbar\Gamma_{10})^2} \right\}, \quad (7)$$

and third-order correction to the RICs can be written as follows:

$$\frac{\Delta n^{(3)}(\omega, I)}{n_r} = -\frac{|M_{10}|^2}{4n_r^3 \varepsilon_0} \frac{\rho \, \mu_0 \, c \, I}{[(E_{10} - \hbar\omega)^2 + (\hbar\Gamma_{10})^2]^2}$$

$$\left[4(E_{10} - \hbar\omega)|M_{10}|^2 - \frac{(M_{11} - M_{00})^2}{(E_{10})^2 + (\hbar\Gamma_{10})^2} \{(E_{10} - \hbar\omega) \right.$$

$$\left. [E_{10}(E_{10} - \hbar\omega) - (\hbar\Gamma_{10})^2] - (\hbar\Gamma_{10})^2(2E_{10} - \hbar\omega)\}\right], \quad (8)$$

where n_r is the relative refractive index of the system, ε_0 and μ_0 stand for vacuum permittivity and permeability, respectively. ρ is the carrier density of the system, ω is the incident photon's angular frequency, I is the optical intensity, $E_{10} = E_1 - E_0$ represents the energy difference of different two electronic states, Γ_{10} is the relaxation rate, and $M_{ij} = \langle \psi_i(z)|e \, z|\psi_j(z) \rangle$ is the dipole moment matrix element. The total ACs and RICs can be given as follows

$$\beta^{(T)}(\omega, I) = \beta^{(1)}(\omega) + \beta^{(3)}(\omega, I) \quad (9)$$

and

$$\frac{\Delta n^{(T)}(\omega, I)}{n_r} = \frac{\Delta n^{(1)}(\omega)}{n_r} + \frac{\Delta n^{(3)}(\omega, I)}{n_r}. \quad (10)$$

3. Results and discussion

In this work, we reported the total AC ($\beta^{(T)}(\omega, I)$) and the total relative RIC ($\Delta n^{(T)}(\omega, I)/n_r$), for a symmetric two-step GaAs/Ga$_{1-x}$Al$_x$As QW, taking into account the third order corrections due to resonant ILF (of intensity I) and the effect of a non-resonant ILF, polarized perpendicularly to the interfaces, for which the dipole approximation applies, and that for sufficiently high frequencies is characterized by the *laser-dressing parameter* α_0 [21], as discussed above in the theoretical framework section.

The system parameters are: $V_0 = 228.0$ meV, the step-like potential width is $L_s = 25$ Å with potential height $V_s = V_0/n$ ($n = 1, 2$ and 4), the well width is set to 50 Å and the central barrier width is $L_{cb} = 30$ Å, with potential height $V_{cb} = 228.0$ meV, as depicted in figure 1(a). In figure 1(b) is reported the potential profile and probability densities, for the ground and first excited states, for $F = 25$ kV cm^{-1}, in figure 1(c) we reported the same system but for $B = 10$ T and finally in figure 1(d) the case of $\alpha_0 = 25$ Å. The resonant laser intensity is $I = 0.4$ MW cm^{-2} [29]. In the next figures we shown first the optical properties of interest as a function of the step-potential height (V_s) and the central barrier width (L_{cb}) (see figure 2), then the effect of electric and magnetic field in figure 3 and finally in figure 4 the non-resonant ILF effect. In the paper's supplementary material (free available online at stacks.iop.org/PS/95/035802/mmedia), we included the energies (E_{10}) and the transition moments (M_{10}) of interest, as functions of B, F and α_0, for a fixed value of the step-like potential profile $V_s = V_0/4$ in order to physically discuss the below described results. In the first case (figure-SM-1(a)), the energy level difference and the dipole matrix element is reported as a function of the applied magnetic field from 0 to 20 T, and the energy difference increases

quadratically from about 12.5 until 15.5 meV while the main dipole matrix element decreases non-monotonously from about 48 until 45 Å that will be reflected in figures 3(a) and (c). The second case (figure-SM-1(b)) corresponds to the above mentioned physical quantities as a function of the electric field (F) from 0 to 50 kV cm^{-1}, but in this case the energy level difference increases almost linearly from 12 until near 50 meV, and the correspondingly dipole matrix element decrease faster than in the previous case, that could be easily observed in figures 3(b) and (d). Finally, the laser dressing parameter dependence (figure-SM-1(c)) is almost parabolic for the main energy difference (E_{10}) and a non-monotonically decreasing dipole matrix element is observed, but in this case the range is wider, so the computed optical changes are more pronounced than in the previous cases, that will be reflected in figures 4(a) and (b). In all the discussed cases, for the chosen ILF intensity of $I = 0.4$ MW cm^{-2}, the third order correction is about 10%, and because the optical properties mainly depend on the main energy transition and on the dipole matrix element, as can be verified from equations (9) and (10) the reported nonlinear optical properties strongly depend on the values of E_{10} and M_{10}, as will be reflected below.

In figure 2 we present the effect of the aluminum concentration x in the step-like potential height (V_s), as well as the central barrier width (L_{cb}), on the AC and the relative RICs for the two-step GaAs/Ga$_{1-x}$Al$_x$As QW. Figure 2(a) shows the total AC for three values of the step-like potential height $V_s = V_0/4$, $V_0/2$ and V_0, the resonant peak undergoes a blue-shift (about 10 meV) and its intensity increases no more than 10% as the V_s value increases, for this particular plot the central barrier width is $L_{cb} = 30$ Å. In figure 2(b) the effect of the central barrier width L_{cb}, considering a step-like potential height of $V_s = V_0/4$, is reported, here the resonant peak experiments a red-shift (also about 10 meV) and the magnitude of the optical AC diminishes as L_{cb} rises. The similar behavior is reported in figures 2(c) and (d) for the relative RICs, the node presents a blue-shift (red-shift) as V_s (L_{cb}) increases. The physical reason for the increase in the AC in figure 2(a) as the step-like potential height increases, for a fixed central barrier width (L_{cb}), is that the overlapping of the involved wave functions increase, and the energy difference between the first excited state and the ground state also does. On the other hand, as the central barrier width (L_{cb}) increases, for a fixed value of the step-like potential height $V_s = V_0/4$, the overlapping decreases causing a diminishing in the AC amplitude, as reported in figure 2(b). Finally, the correspondingly relative RICs also responds to the dipole matrix element behavior.

In figure 3 are shown the effect of the magnetic and electric fields on the total AC and the total relative RIC, that includes the linear and third-order correction due to the incident optical intensity I. In all the reported cases the step-like potential is set to $V_s = V_0/4$ and the central barrier width is 25 Å with a barrier height V_0 and the laser dressing parameter $\alpha_0 = 0$. In figure 3(a) is reported the AC, without any electric field, for magnetic field values of 0, 10 and 20 T, and in can be seen that the resonant peak becomes lightly blue-shifted in energy, from 13.5 meV ($B = 0$) to 16.5 meV
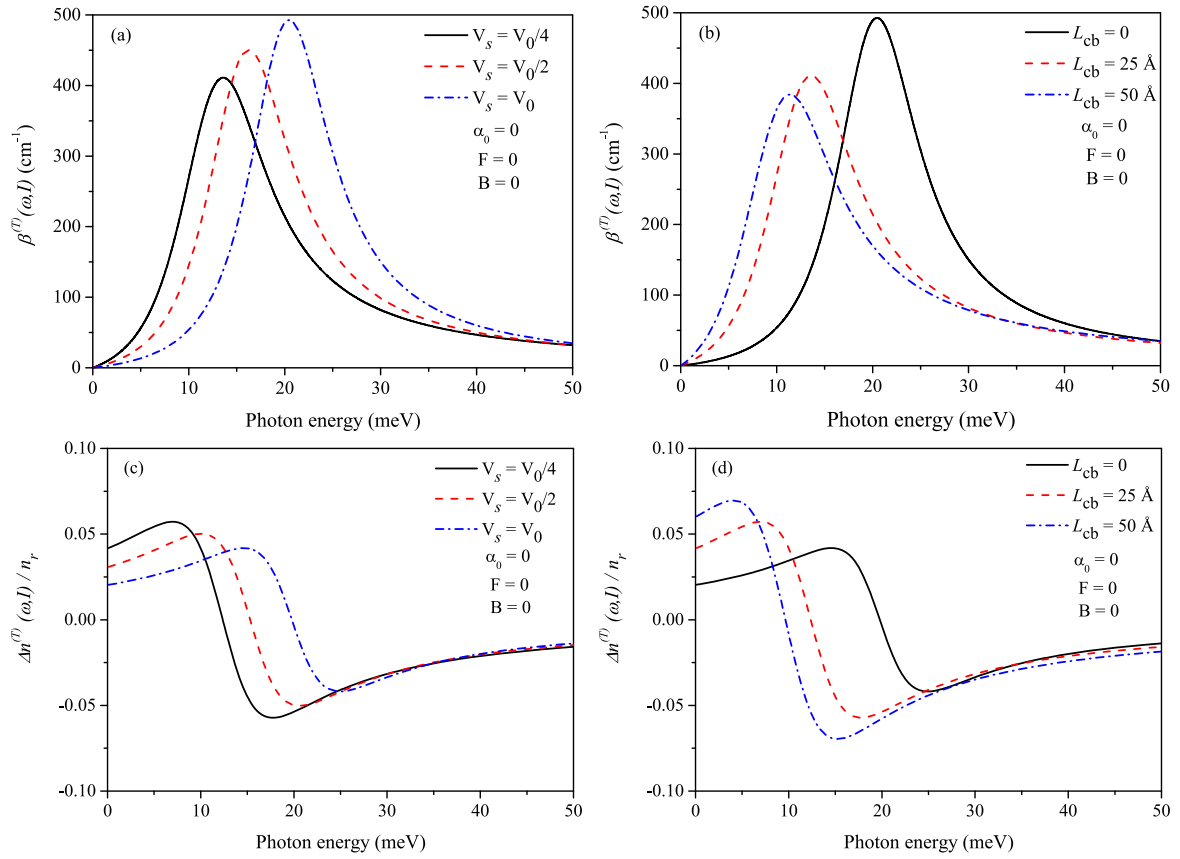
Figure 2. Absorption coefficient (a), (b) and relative refractive index changes (c), (d) for the two-step GaAs/Ga$_{1-x}$Al$_x$As quantum well, considering different values of the step-like potential height V_s (a), (c) and the central barrier width L_{cb} (b), (d). We found that those structural parameters shift the energy and magnitude of the optical properties.

($B = 20\,\text{T}$), and also increases slightly in its magnitude. In 3(b), turning off the magnetic field, and considering the electric field effect it can be seen a more pronounced blue-shift with a significant decrease in the AC magnitude, for instance for $F = 0$ the AC resonant peak is at 13.5 meV with an amplitude of $410\,\text{cm}^{-1}$, when $F = 25\,\text{kV}\,\text{cm}^{-1}$ the AC energy is 27 meV and finally when $F = 50\,\text{kV}\,\text{cm}^{-1}$ the resonant peak is at 49 meV but with a 60% decrease in magnitude. The same general behavior holds for the relative RIC reported in figures 3(a) and (b) a light blue-shift of the node for the magnetic field and the more important node blue-shift for the applied electric field case. We compared our results with the available data reported in the literature, for instance in [14] they reported an intersubband optical absorption coefficient for a double QW structure, with comparable dimensions to our system, with resonant peak around 30 μm (about 40 meV), our results (see figure 3(b)) are in good agreement with the above-mentioned reference.

Finally, in figure 4 we reported the effect of the non-resonant ILF through the laser dressing parameter α_0 with values of 0, 25 and 50 Å, considering fixed values for the step-like potential barrier $V_s = V_0/4$ and for the central barrier width (L_{cb}) of 25 Å without any applied electromagnetic field. In general we found that, as the value of α_0 increases, the total AC ($\beta^{(T)}(\omega, I)$) experiences a blue-shift, and its amplitude also increases. For instance, when $\alpha_0 = 0$ the total

AC has a magnitude of about $400\,\text{cm}^{-1}$ and the resonant peak is located about 15 meV. When the value of $\alpha_0 = 25$ Å the resonant peak is now about 20 meV and its amplitude increases almost 50%. And for a value of $\alpha_0 = 50$ Å the total AC peak is about 55 meV and its amplitude increases almost 110%, with respect to the non applied intense laser ($\alpha_0 = 0$), reaching about $880\,\text{cm}^{-1}$ in its maximum. In the case of the computed total relative RIC ($\Delta n^{(T)}(\omega, I)/n_r$), as the laser dressing parameter increases, the nodes of this are blue-shifted and its amplitude diminishes, as reported in figure 4(b). The total relative RIC diminishes almost 50% for $\alpha_0 = 50$ Å, compared with non-applied ILF effect ($\alpha_0 = 0$). All the previous discussion could be of great importance for possible applications as photodetectors or, when the asymmetry increases by electric fields, this particular heterostructure could be considered as an active region for QCL, as discussed in the introduction section.

4. Conclusions

In this paper we computed the AC and the relative RIC considering the third order correction for a symmetric two-step GaAs/Ga$_{1-x}$Al$_x$As QW. The system was subjected to the presence of a constant electric field along the growth direction z, to an in-plane (x-directed) constant magnetic field
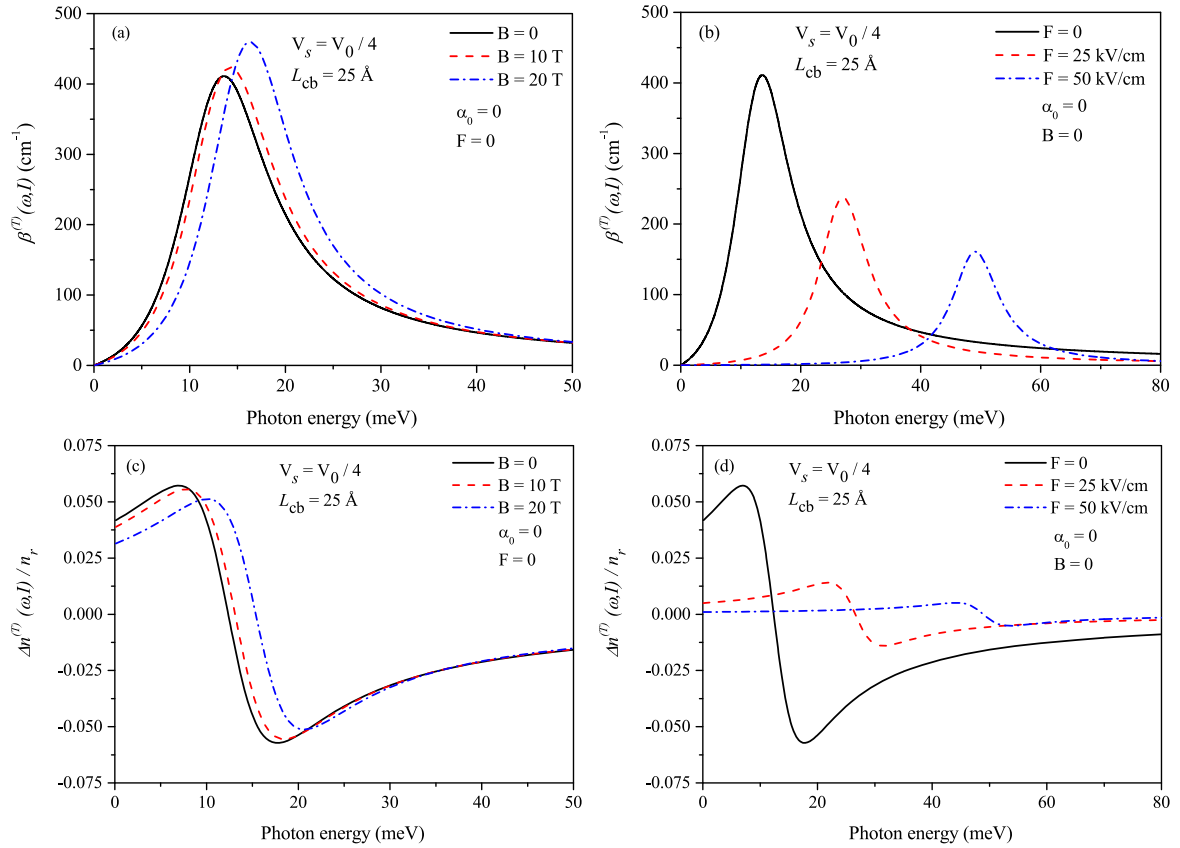
Figure 3. Effect of the magnetic and electric fields on the nonlinear optical properties of interest for the system. In (a) and (b) are shown the total absorption coefficient for magnetic field of 0, 10 T and 20 T, and electric fields of 0, 25 kV cm^{-1} and 50 kV cm^{-1}, respectively. In (c) and (d) are shown the total relative refractive index chance, for the same magnetic and electric field values. In all cases the step-like potential is set to $V_s = V_0/4$ and the central barrier width is 25 Å with $\alpha_0 = 0$.
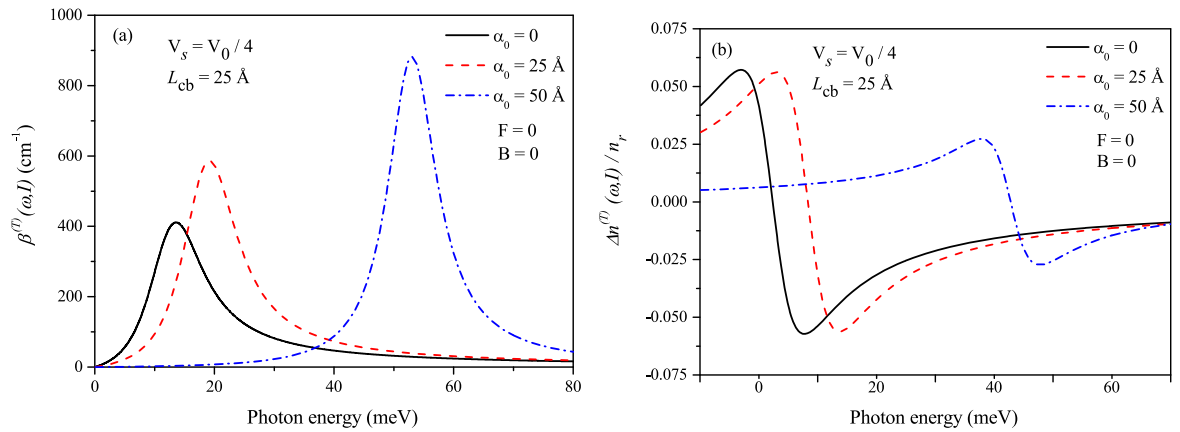
Figure 4. Total absorption coefficient ($\beta^{(T)}(\omega, I)$) and total relative refractive index change ($\Delta n^{(T)}(\omega, I)/n_r$) for the system as a function of the laser dressing parameter $\alpha_0 = 0$, 25 and 50 Å, and a step potential $V_s = V_0/4$ with a central barrier width (L_{cb}) of 25 Å, without any applied electric and magnetic fields.

B and also to the effect a non-resonant ILF characterized by the laser-dressing parameter α_0. The results show that when the values of the step-like potential profile and the central barrier width increase, the AC and the relative RIC undergo a small blue-shift and a red-shift, respectively, and their magnitude decreases by approximately 10%. We have a blue-shift in the optical properties as the electric and magnetic field values both rise. Also, the magnitude of the AC and relative

RIC increases and diminishes, respectively, as the magnetic field increases. The magnitude of both optical properties decreases as the values of the electric field increase. For the non-resonant ILF, the AC and the relative RIC experiment a more meaningful blue-shift and the magnitude -increases about almost 110% by the AC- and decreases the index change about 50%, relatively to the absence of the ILF. In general, we found that the studied optical properties can be

tuned by system parameters or applying external factors, as discussed here.

Acknowledgments

ORCID iDs

J C Martínez-Orozco https://orcid.org/0000-0001-8373-1535
F Ungan https://orcid.org/0000-0003-3533-4150
K A Rodríguez-Magdaleno https://orcid.org/0000-0002-0749-3931

References

[1] Zhang Y, Gu Y, Chen P, Zhang Y, Zheng Y, Yu C, Li X and Gong H 2018 *Mater. Sci. Semicond. Proc.* **79** 107
[2] Cetinkaya C, Cokduygulular E, Nutku F, Donmez O, Puustinen J, Hilska J, Erol A and Guina M 2018 *J. Alloys Compd.* **739** 987
[3] Yue L, Song Y, Chen X, Chen Q, Pan W, Wu X, Liu J, Zhang L, Shao J and Wang S 2017 *J. Alloys Compd.* **695** 753
[4] Pierścińska D, Gutowski P, Hałdaś G, Kolek A, Sankowska I, Grzonka J, Mizera J, Pierściński K and Bugajski M 2018 *Semicond. Sci. Technol.* **33** 035006
[5] Brandstetter M, Kainz M A, Zederbauer T, Krall M, Schönhuber S, Detz H, Schrenk W, Andrews A M, Strasser G and Unterrainer K 2016 *Appl. Phys. Lett.* **108** 011109
[6] Lin T T and Hirayama H 2018 *Phys. Status Solidi* a **215** 1700424
[7] Liu G, Guo K, Zhang Z, Hassanbadi H and Lu L 2018 *Thin Solid Films* **662** 27
[8] Sahoo N, Panda A K and Sahu T 2017 *Phys. Status Solidi* b **254** 1700221
[9] Martínez-Orozco J, Rojas-Briseño J, Rodríguez-Magdaleno K, Rodríguez-Vargas I, Mora-Ramos M, Restrepo R, Ungan F, Kasapoglu E and Duque C 2017 *Physica* B **525** 30
[10] Dakhlaoui H 2015 *J. Appl. Phys.* **117** 135705
[11] Ungan F, Yesilgul U, Sakiroglu S, Kasapoglu E, Sari H and Sökmen I 2013 *J. Lumin.* **143** 75
[12] Karabulut İ, Mora-Ramos M E and Duque C A 2011 *J. Lumin.* **131** 1502
[13] Palo S K, Sahu T and Panda A 2018 *Physica* B **545** 62
[14] Zhang W, Wang Z and Ban S 2018 *J. Semicond.* **39** 122002
[15] Kasapoglu E, Duque C A, Mora-Ramos M E, Restrepo R L, Ungan F, Yesilgul U, Sari H and Sökmen I 2015 *Mater. Chem. Phys.* **154** 170
[16] Song Y F, Zhu Q S, Liu X L, Yang S Y and Wang Z G 2015 *Int. J. Mod. Phys.* B **29** 1550212
[17] Tang C and Shi J 2015 *Physica* E **69** 96
[18] Rojas-Briseño J G, Martínez-Orozco J C and Mora-Ramos M E 2017 *Superlattices Microstruct* **112** 574
[19] Liu D and He C 2018 *J. Comput. Electron.* **18** 251
[20] Dakhlaoui H 2018 *Optik* **168** 416
[21] Lima F M S, Amato M A, Nunes O A C, Fonseca A L A, Enders B G and da Silva E F Jr 2009 *J. Appl. Phys.* **105** 123111
[22] Ungan F, Kasapoglu E, Duque C A, Yesilgul U, Şakiroglu S and Sökmen I 2011 *Eur. Phys. J.* B **80** 89
[23] Duque C A, Kasapoglu E, Şakiroglu S, Sari H and Sökmen I 2011 *Appl. Surf. Sci.* **257** 2313
[24] Panda M, Das T and Panda B K 2018 *Int. J. Mod. Phys.* B **32** 1850032
[25] Sari H, Ungan F, Sakiroglu S, Yesilgul U and Sökmen I 2018 *Optik* **162** 76
[26] Niculescu E 2017 *Opt. Mater.* **64** 540
[27] Aktas S, Kes H, Boz F and Okan S 2016 *Superlattices Microstruct.* **98** 220
[28] Sakiroglu S, Yesilgul U, Ungan F, Duque C, Kasapoglu E, Sari H and Sokmen I 2012 *J. Lumin.* **132** 1584
[29] Boyd Robert W. 2008 *Nonlinear Optics* 3rd edn (London: Academic Press) 9780123694706